Collective mode splitting in hybrid heterostructures

Juan Gabriel Ramírez,[1,2] J. de la Venta,[3] Siming Wang,[1,4] Thomas Saerbeck,[5] Ali C. Basaran,[1,6] X. Batlle,[7] and Ivan K. Schuller[1,*]

[1]*Department of Physics and Center for Advanced Nanoscience, University of California San Diego, La Jolla, California 92093, USA*

[2]*Department of Physics, Universidad de los Andes, Bogotá 111711, Colombia*

[3]*Department of Physics, Colorado State University, Fort Collins, Colorado 80523, USA*

[4]*Materials Science Division, Lawrence Berkeley National Laboratory, Berkeley, California 94720, USA*

[5]*Institut Laue-Langevin, 71 avenue des Martyrs, 38000 Grenoble, France*

[6]*Department of Physics, Gebze Technical University, Gebze, Kocaeli 41400, Turkey*

[7]*Departament de Física de la Matèria Condensada and Institut de Nanociència i Nanotecnologia Universitat de Barcelona, 08028 Barcelona, Catalonia, Spain*

(Received 1 November 2015; revised manuscript received 26 May 2016; published 21 June 2016)

We report on a drastic change of the Ni collective magnetization dynamics when incorporated into a Ni/V_2O_3 heterostructure. Two, unexpected, well-defined Ni ferromagnetic resonance (FMR) modes are observed in the coexistence region of the first-order V_2O_3 structural phase transition (SPT). The phase coexistence across the V_2O_3 SPT can explain the presence of the two resonance fields but not their anticrossing and large linewidth broadenings. Our results imply a strong coupling between the lattice dynamics of the strongly correlated oxide (V_2O_3) and the magnon modes of the ferromagnet (Ni) in this hybrid. This and additional experiments on Ni grown on $SrTiO_3$, a prototypical second-order phase transition oxide, imply that these effects require the presence of first-order transitions in the oxides.

DOI: 10.1103/PhysRevB.93.214113

Novel functionalities can be achieved in hybrid materials by the coupling of electronic, magnetic, and structural properties between the constituents when they are in close physical proximity [1,2]. For example, quasistatic magnetic properties of conventional ferromagnets can be controlled via piezoelectric [3] or multiferroic materials [4]. Recently, it was shown that first-order structural phase transitions (SPTs) of proximal transition metal oxides drastically influence the *static* magnetic properties [5,6]. On the other hand, the dynamical properties of the magnetization, i.e., the dispersion of spin waves or magnons across the SPT of a proximal layer, have not been explored. The collective modes in the ferromagnetic layer of a hybrid heterostructure may couple to other collective modes, such as phonons [7–12], which may lead to new physics and enhanced functionalities. Therefore, incorporation of ferromagnets and materials with SPTs into a single hybrid structure opens up a new avenue for tuning the magnetization dynamics and the creation of novel properties in artificially designed hybrid materials. An example of this type of hybrid materials is a Nickel film in contact with Vanadium sesquioxide (V_2O_3), which undergoes a first-order SPT, a metal-insulator transition (MIT) and an antiferromagnetic phase transition in the temperature range of 150–160 K [13,14]. The volume change across the SPT is around 1%, and complex phase coexistence has been shown to affect the static magnetism of a proximal ferromagnetic material [13].

In this letter, we report on a drastic modification of the magnetization dynamics of a Ni thin film caused by the first-order SPT of a proximal V_2O_3 thin film. We found that the typical out-of-plane uniform ferromagnetic resonance (FMR) mode of Ni splits into two distinct modes in the temperature region of the V_2O_3 SPT. The two resonances change proportionally to the phase fraction evolution of V_2O_3 and the related laterally differently strained Ni in the heterostructure. However, the resonance field shifts (anticrossing), and linewidth changes are completely unexpected and cannot be accounted by the phase coexistence. This shows that mode splitting and anticrossing can occur even if the collective modes are located in different spatial locations. The origin of this behavior is related to coupling to other collective modes possibly soft phonon modes. These conclusions are based on extensive x-ray diffraction (XRD), low-temperature scanning electron microscopy (SEM), scattering-type scanning near-field optical microscopy (s-SNOM), temperature, angle, the use of different materials, buffer layers, and substrates (many presented in the Supplemental Material [15]).

V_2O_3 thin films (100 nm thick) were deposited by radio frequency (RF) magnetron sputtering of a V_2O_3 target (>99.7% purity, ACI Alloys, Inc.) on *R*-plane sapphire substrates at 750 °C. The sputtering chamber has a base pressure of 1×10^{-7} Torr. During sputtering, 4 mTorr ultrahigh purity (UHP) Ar and 100 W RF forward power were used. After V_2O_3 deposition, the substrate was cooled to 25 °C for the deposition of 10 nm Ni and 7 nm Nb as capping layer. The thickness and structural morphology of the individual layers were measured by x-ray reflectometry (XRR) and XRD ($\lambda_{CuK\alpha} = 1.54$ Å) (in and out of plane) as a function of temperature. The Ni roughness obtained from the refinement of XRR is 1.3 nm, mostly determined by the interface with the oxide (2 nm roughness). The XRD confirmed epitaxial single-phase growth of V_2O_3. The SPT of the V_2O_3 film from a rhombohedral (012) to monoclinic (011) crystal structure is characterized by a shift of the out-of-plane diffraction peak, giving a change of the out-of-plane lattice constant from $d_{(012)} = 3.66$ Å at 300 K to $d_{(011)} = 3.70$ Å at 100 K [6,13,16]. See Supplemental Material for details on the XRR and XRD [15].

*Corresponding author: ischuller@ucsd.edu

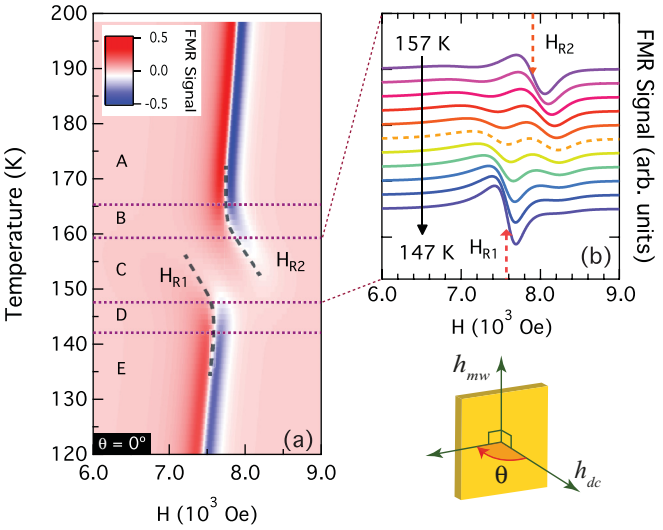

FIG. 1. (a) Contour plot of the out-of-plane FMR signal ($\theta = 0^\circ$) as a function of dc magnetic field at different temperatures from 200 K to 120 K. The horizontal dotted lines indicate different temperature regions (A–E), and the dashed lines indicate H_{R1} and H_{R2}. (b) The FMR signal from 157 K to 147 K [region C in (a)] with 1 K steps. The dashed line corresponds to the center of the SPT at 152 K. Curves are shifted vertically for clarity. Vertical arrows indicate the resonance fields H_{R1} at 147 K and H_{R2} at 157 K. The sketch depicts the sample geometry used in the measurements: The dc magnetic field, $h_{\rm dc}$, is perpendicular to the sample surface, and the microwave field $h_{\rm mw}$ is in the plane. The arrow indicates the angle increase direction from out of plane to in-plane.

The FMR was measured using a Bruker EleXsys EPR spectrometer with a cylindrical cavity resonator at 9.4 GHz connected to a liquid helium flow-cryostat in the 3.8 to 300 K temperature range. The effect of the V_2O_3 SPT on the FMR was monitored at temperature intervals of 1 K between 200 K and 100 K while cooling. At each step the temperature was stabilized within ± 0.1 K. The samples, placed in the center of the cavity, were mounted on a quartz rod allowing for in- and out-of-plane orientation of the dc magnetic field (see sketch in Fig. 1). An automatic goniometer allowed for precise rotation with an accuracy of $\Delta\theta = 0.025^\circ$. Alignment of the sample with respect to the ac and dc fields was performed by finding the highest resonant field while rotating the sample about the out-of-plane direction ($\theta = 0^\circ$) within 0.2°. This procedure was repeated at 100 K and 300 K to account for changes in the alignment due to thermal expansion. The dc magnetic field was swept from 0 to 9000 Oe at 60 Oe s^{-1}. The microwave power was kept constant at 10 mW in order to increase the signal-to-noise ratio. Similar results were obtained with microwave powers as low as 0.1 mW. The linewidth (ΔH), peak-to-peak distance, and the resonance field (H_R), the field at zero crossing from positive to negative signal were obtained by fitting the FMR signal to the derivative of a Lorentzian function. Analyses of the resonant field and the extracted anisotropy constants from the main FMR (uniform) mode as a function of the temperature are discussed in the Supplemental Material [15].

The temperature dependent FMR measurements are summarized in the contour plot Fig. 1(a). From 200 K to 165 K, a single resonance mode is observed and the associated resonance field decreases monotonically (region A). Below 165 K, the resonance field shifts to higher values by 60 Oe in region B. In the center of the SPT (region C), the FMR signal splits into two well-defined modes. The resonance field H_R of each mode increases with decreasing temperature in this central region and shows an anticrossinglike behavior [gray dash lines in Fig. 1(a)]. The FMR signal in this region is shown for selected temperatures in Fig. 1(b) with two resonance modes observed at H_{R1} and H_{R2}. Below 147 K, a single FMR mode is recovered [Fig. 1(a), region D], and the resonant field resumes the decreasing trend with decreasing temperature. The low (region D) and high (region A and B) temperature regions were fitted using the derivative of a single Lorentzian function, while for the intermediate temperatures (157 to 147 K, region C) we used derivatives of two Lorentzian functions (for details about the fitting procedure see the Supplemental Material [15]).

The temperature dependences of H_R and ΔH extracted from the fits are summarized in Fig. 2. The resonance field in Fig. 2(a) represents the cooling branch, as indicated by the arrow. For comparison, resonance fields extracted from the fits to the FMR signal of a 10 nm Nickel film grown directly on R-plane sapphire substrate under similar conditions are included in Fig. 2(a) (open green squares). At 200 K, the resonant field for the Ni film is 80 Oe smaller than for the Ni/V_2O_3 bilayer possibly due to different roughness [1,2,17], which is on the order of 0.5 nm for a 10 nm Ni film on Al_2O_3 substrate. For all temperatures measured, the H_R of the Ni film shows a linear decrease with decreasing temperature.

The FMR linewidths obtained from the fits are shown in Fig. 2(b) for the Ni/V_2O_3 bilayer and the Ni reference film. In the bilayer, the FMR linewidth is 128 Oe at 200 K and remains constant until 165 K (region A). With further decreasing temperature, the linewidth increases (region B), reaching 264 Oe at 160 K, a 67% increase above that at 166 K. Once the FMR mode splitting takes place (region C), the linewidths (ΔH_1, ΔH_2) associated with each resonance (H_{R1}, H_{R2}) show a maximum at different temperatures. ΔH_1 reaches a maximum of 831 Oe at 158 K, while ΔH_2 increases to 345 Oe at 154 K. The linewidth of H_{R2} below the SPT (region E) remains slightly higher (approximately 40 Oe) compared to ΔH_1 above the SPT (region A). In contrast, the linewidth of the single Ni film is temperature independent between 300 K and 100 K [green open squares in Fig. 2(b)] with a value close to that of the Ni/V_2O_3 bilayer above the SPT.

The temperature region with a coexistence of two V_2O_3 crystallographic phases during the transition can be obtained from the temperature dependent XRD [13]. Two vertical dotted red lines in Fig. 2 indicate the coexistence region of the two phases extracted from Fig. 3. Remarkably, the width of the SPT coincides with the region in which the resonance field and linewidth of Ni film deviates from the behavior of a single Ni film of similar thickness [Fig. 2(a), regions B, C, and D]. Furthermore, XRR measurements as a function of the temperature reveal no changes in the $Nb/Ni/V_2O_3$ layer structure and suggest no significant change in the interface roughness and grain morphology along the out-of-plane direction across the SPT (see Supplemental Material [15]). Therefore, we can conclude that the existence of two well-defined collective

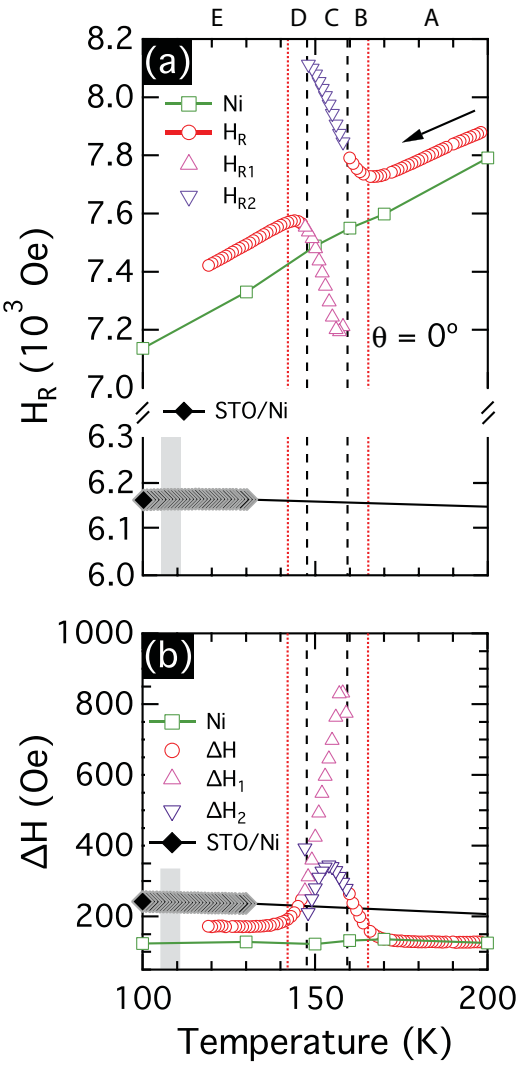

FIG. 2. (a) Temperature dependence of the resonance field H_R across the SPT of V_2O_3. Letters on top correspond to the temperature regions in Fig. 1(a). (b) Temperature dependence of the linewidth ΔH. Data in (a) and (b) are extracted from fits to the data. H_R and ΔH for 10 nm Ni deposited on R-cut sapphire and $SrTiO_3$ substrates are shown at selected temperatures (green open symbols for Ni and black solid symbols for $SrTiO_3$/Ni). The gray area at 105 K corresponds to the STO phase transition region. Dotted vertical lines correspond to the V_2O_3 SPT phase coexistence region as measured by the temperature dependent x-ray diffraction. Dashed vertical lines indicate the region of the splitting of the FMR mode [region C in Fig. 1(a)].

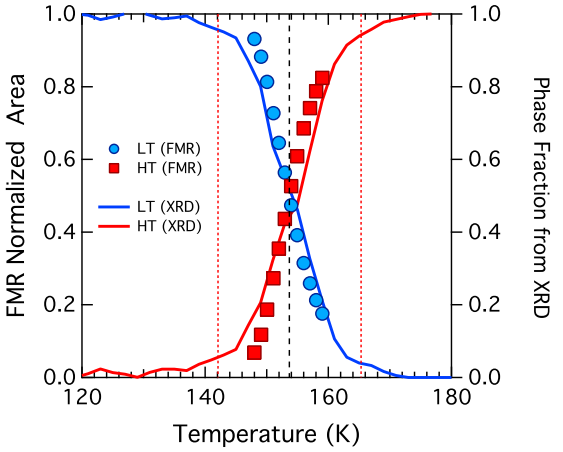

FIG. 3. Normalized peak intensity for the two resonances observed across the SPT. LT (HT) corresponds to low (high) temperature phase fraction. The vertical dashed line depicts the temperature of the crossing point at which both intensities are equal (154 K). The continuous lines (red and blue) correspond to the phase fraction obtained from the temperature dependent out of plane XRD measurements. The vertical dotted lines indicate the same temperature range as in Fig. 2.

modes is due to the V_2O_3 crystallographic phase coexistence, typical of first-order phase transitions.

As a control experiment we deposited a 10 nm Ni film on a $SrTiO_3$ (STO) substrate. The second-order displacive phase transition of STO at 105 K [18] involves a rotation of TiO_6 octahedra and has been regarded as a classic example of a soft-mode-induced phase transition [19]. Thus, no phase coexistence is expected nor found across the SPT of STO. The resonant field and linewidth are plotted in Fig. 2 (black solid symbols). These results across the SPT of STO (gray region in Fig. 2) show no indication of the behavior described above. This reinforces the conclusion that the spatial phase coexistence of the first-order transition is the source of the two resonances observed in Ni/V_2O_3 bilayers. The absence of any temperature dependence of the resonant field and linewidth suggest a small crystalline anisotropy compared with Ni on the R-cut sapphire substrate or in the case of V_2O_3/Ni samples.

Additional control experiments were performed in Nb/Ni/V_2O_3 with thicker Ni layers and Nb/Ni/Cu/V_2O_3 heterostructures. We observed that for thick Ni films, the splitting of the FMR modes becomes less evident for thicknesses above 100 nm. Insertion of a Cu layer into Nb/Ni/Cu/V_2O_3 heterostructures was used to decouple a possible magnetic effect arising from interfacial magnetic coupling between the Ni film and the antiferromagnetic phase of V_2O_3 below the SPT. We found that the mode splitting persists for Cu thicknesses up to 20 nm if the Ni layer is kept constant at 10 nm.

In general, the temperature dependence of the resonance field of a magnetic thin film is determined by the magnetocrystalline anisotropy and the magnetization [1]. This gives rise to the expected reduction of H_R with decreasing temperature in the reference Ni film for all temperatures and for the bilayer Ni/V_2O_3 above and below the V_2O_3 SPT [Fig. 2(a)]. Therefore, our results in the temperature region outside the SPT are consistent with early results for single highly oriented Ni thin films [5,20,21] and with the behavior of the Ni reference samples.

In contrast to the linear temperature dependence above and below the SPT, the two resonance modes across the V_2O_3 transition cannot be explained using additional terms in the anisotropy of a *homogeneous* Ni film (see Supplemental Material [15]). Instead, the presence of two well-defined resonances arises naturally from the existence of two different and spatially separated anisotropies in the same sample, similar to the presence of two ferromagnetic materials or a photonic crystal [22,23]. This implies that the coexistence of two phases across the V_2O_3 SPT produces two well-defined anisotropies in

the Ni film. This agrees with the static magnetometry [5,6,13]. Figure 3 shows the normalized areas of the two deconvoluted Lorentzian obtained from a fit of the FMR (see Supplemental Material [15]). The low temperature FMR mode, arising from the nucleation of monoclinic V_2O_3, grows at the expense of the high temperature mode related to the rhombohedral V_2O_3 phase. At maximum phase coexistence (50% of each phase), two resonance modes of equal intensity are observed (dashed line in Fig. 3 at 152 K). This behavior of the FMR intensities coincides with the relative phase fraction extracted from the XRD across SPT of V_2O_3 (Fig. 3) (see Supplemental Material [15]). This model, in which two crystallographic domains across the SPT produce two well-defined anisotropies in the Ni explains the appearance of two collective modes and their intensity evolution in the V_2O_3 coexistence region. The splitting of collective modes implies regions of the two anisotropies that are laterally well separated. Microscopy investigations of the SPT of V_2O_3 indicated nucleation sites of 100 nm diameter [24,25], which can be approximated as the magnetic domain of altered anisotropy. Despite the direct proximity of the two domains, the modes do not average and appear to act as independent materials. This is in direct contrast to, for example, the observation of a single, averaged transition in metallic heterostructures, which only show two distinct ac susceptibilities upon separation [26].

On the other hand, the repulsion (anticrossing) of the two resonance modes and the inverted temperature dependence of the resonance fields [see Figs. 1(a) and 2(a)] across SPT cannot be explained by the phase coexistence and implies the existence of new physics. In a more general way, the mode splitting observed is reminiscent of the topology of the von Neumann–Wigner noncrossing rule [27]. Avoided crossings are a common observation in quantum mechanics of coupled oscillators, for example, between phononic or electronic states of same symmetry [28]. Consequently, the two FMR modes must be coupled to each other, either directly or by indirect coupling over the lattice of the oxide, which is further enhanced by the SPT. This coupling may be estimated to be weak since the two modes do not average into a single collective mode. To our knowledge, no observation of avoided crossings in magnonic systems with laterally inhomogeneous anisotropies has ever been reported. In coupled piezoelectric/ferromagnetic heterostructures only a shift in resonance field and no significant change in linewidth are observed [3].

The linewidth is attributed to loss processes and magnon relaxation. In ferromagnetic metals these are commonly related to spin-orbit coupling [29,30], which depends only weakly on the temperature. Thus, the linewidth of the single Ni film is constant from 300 K down to 100 K. In the Ni/V_2O_3, on the other hand, the difference in linewidth between 200 K and 100 K indicates enhanced dissipation (decreased relaxation time) at low temperatures. These changes point to an altered magnetic damping and additional relaxation mechanisms arising due to the SPT, which indicates new physics. The importance of phase coexistence is implied by the linewidth increase shown in Fig. 2(b). The strong increase of the Ni linewidth at the SPT of V_2O_3 indicates that spatial crystallographic disorder is responsible for the additional dissipation since it coincides with the temperature at which there is maximum two-phase coexistence. Additional relaxation mechanisms could arise from more complex magnon-lattice coupling due to spatial variations in the lattice, anisotropy, and magnetization fields [31]. For instance, two-magnon processes [32,33] or inhomogeneous line broadening [34] are related to the presence of intrinsic or extrinsic disorder. Both observed modes in the Ni/V_2O_3 transition region show line broadening, therefore indicating that each domain shows a disordered substructure on smaller length scales, either intrinsic within the domains or at their boundary [34]. While disorder is the most likely cause of the increased losses, the detailed underlying mechanism is yet unclear and requires further detailed studies, for example, by investigating the frequency dependence of each FMR mode.

In summary, we showed that the phase coexistence of the first-order phase transition of an oxide strongly modifies the collective spin dynamics of a proximity coupled ferromagnetic layer. Our results imply strong coupling between the lattice dynamics of a strongly correlated oxide and the magnon spectra of the proximal ferromagnet. The phase coexistence across the V_2O_3 SPT can explain the presence of two resonance fields but not their anticrossing and large nonmonotonic linewidth broadening. The absence of similar effects in Ni/STO suggests that phase coexistence and disorder of a first-order SPTs are essential for the observation of these effects. We showed that the evolution of the FMR modes throughout the SPT allows access to underlying strain, disorder, and spatial coupling energies. Our results also open up a new avenue for the manipulation of magnetization dynamics by the incorporation of materials into properly designed hybrid heterostructures.

We acknowledge fruitful discussions with Axel Hoffmann, Bekir Aktas, and M. R. Fitzsimmons. The magnetism aspects of this paper were supported by the Office of Basic Energy Science, U.S. Department of Energy, under Grant No DE FG02-87ER-45332, and the oxide related science by the Air Force Office of Scientific Research (AFOSR) Grant No. FA9550-12-1-0381. J.G.R. kindly acknowledges support from the FAPA program through the Facultad de Ciencias and Vicerrectoria de Investigaciones of the Universidad de los Andes, Bogotá Colombia. X.B. acknowledges the support of the Spanish Ministry of Economy and Competitiveness (MINECO) (No. MAT2015-68772-P), Catalan Ministry of Universities, Research and Information Society (DURSI) (No. 2009SGR856 and No. 2014SGR220), European Union Fondo Europeo de Desarrollo Regional (FEDER) funds (Una manera de hacer Europa), and the University of Barcelona. I.K.S. thanks the U.S. Department of Defense for a National Security Science and Engineering Faculty Fellowship (NSSEFF).

[1] C. Kittel, Phys. Rev. **73**, 155 (1948).

[2] H. Y. Hwang, Y. Iwasa, M. Kawasaki, B. Keimer, N. Nagaosa, and Y. Tokura, Nat. Mater. **11**, 103 (2012).

[3] M. Weiler, A. Brandlmaier, S. Geprägs, M. Althammer, M. Opel, C. Bihler, H. Huebl, M. S. Brandt, R. Gross, and S. T. B. Goennenwein, New J. Phys. **11**, 013021 (2009).

[4] Z. Zhou, M. Trassin, Y. Gao, Y. Gao, D. Qiu, K. Ashraf, T. Nan, X. Yang, S. R. Bowden, D. T. Pierce, M. D. Stiles, J. Unguris, M. Liu, B. M. Howe, G. J. Brown, S. Salahuddin, R. Ramesh, and N. X. Sun, Nat. Commun. **6**, 6082 (2015).
[5] J. de la Venta, S. Wang, J. G. Ramirez, and I. K. Schuller, Appl. Phys. Lett. **102**, 122404 (2013).
[6] T. Saerbeck, J. de la Venta, S. Wang, J. G. Ramírez, M. Erekhinsky, I. Valmianski, and I. K. Schuller, J. Mater. Res. **29**, 2353 (2014).
[7] G. T. Hohensee, R. B. Wilson, J. P. Feser, and D. G. Cahill, Phys. Rev. B **89**, 024422 (2014).
[8] C. Kittel, Phys. Rev. **110**, 836 (1958).
[9] E. Schlömann, J. Appl. Phys. **31**, 1647 (1960).
[10] L. Graf and G. Schaack, Z. Phys. B **24**, 83 (1976).
[11] R. Weber, Phys. Rev. **169**, 451 (1968).
[12] R. Valdés Aguilar, A. B. Sushkov, C. L. Zhang, Y. J. Choi, S.-W. Cheong, and H. D. Drew, Phys. Rev. B **76**, 060404 (2007).
[13] J. de la Venta, S. Wang, T. Saerbeck, J. G. Ramirez, I. Valmianski, and I. K. Schuller, Appl. Phys. Lett. **104**, 062410 (2014).
[14] S. Lupi, L. Baldassarre, B. Mansart, A. Perucchi, A. Barinov, P. Dudin, E. Papalazarou, F. Rodolakis, J. P. Rueff, J. P. Itié, S. Ravy, D. Nicoletti, P. Postorino, P. Hansmann, N. Parragh, A. Toschi, T. Saha-Dasgupta, O. K. Andersen, G. Sangiovanni, K. Held, and M. Marsi, Nat. Commun. **1**, 105 (2010).
[15] See Supplemental Material at http://link.aps.org/supplemental/10.1103/PhysRevB.93.214113 for a detailed description of the XRD and XRR.
[16] J. G. Ramirez, T. Saerbeck, S. Wang, J. Trastoy, M. Malnou, J. Lesueur, J.-P. Crocombette, J. E. Villegas, and I. K. Schuller, Phys. Rev. B **91**, 205123 (2015).
[17] M. T. Johnson, P. J. H. Bloemen, F. J. A. den Broeder, and J. J. de Vries, Rep. Prog. Phys. **59**, 1409 (1996).
[18] E. K. H. Salje, M. Guennou, P. Bouvier, M. A. Carpenter, and J. Kreisel, J. Phys.: Condens. Matter **23**, 275901 (2011).
[19] S. Singh, T.-Y. Chien, J. R. Guest, and M. R. Fitzsimmons, Phys. Rev. B **85**, 115450 (2012).
[20] N. Jedrecy, H. J. von Bardeleben, V. Badjeck, D. Demaille, D. Stanescu, H. Magnan, and A. Barbier, Phys. Rev. B **88**, 121409 (2013).
[21] C. Zener, Phys. Rev. **96**, 1335 (1954).
[22] C. Yu, M. J. Pechan, and G. J. Mankey, Appl. Phys. Lett. **83**, 3948 (2003).
[23] M. Krawczyk and D. Grundler, J. Phys.: Condens. Matter **26**, 123202 (2014).
[24] A. S. McLeod, E. v. Heumen, J. G. Ramirez, S. Wang, T. Saerbeck, S. Guenon, M. Goldflam, L. Anderegg, P. Kelly, A. Mueller, M. Liu, I. K. Schuller, and D. N. Basov (unpublished) (2016).
[25] S. Guenon, S. Scharinger, S. Wang, J. G. Ramirez, D. Koelle, R. Kleiner, and I. K. Schuller, Europhys. Lett. **101**, 57003 (2013).
[26] U. Bovensiepen, F. Wilhelm, P. Srivastava, P. Poulopoulos, M. Farle, A. Ney, and K. Baberschke, Phys. Rev. Lett. **81**, 2368 (1998).
[27] J. von Neumann and E. Wigner, Phys. Z. **30**, 467 (1929).
[28] L. V. Abdurakhimov, Y. M. Bunkov, and D. Konstantinov, Phys. Rev. Lett. **114**, 226402 (2015).
[29] C. E. Patton, J. Appl. Phys. **39**, 3060 (1968).
[30] M. J. Hurben and C. E. Patton, J. Appl. Phys. **83**, 4344 (1998).
[31] H. Suhl, IEEE Trans. Magn. **34**, 1834 (1998).
[32] D. L. Mills and S. Rezende, in *Spin Dynamics in Confined Magnetic Structures II*, edited by B. Hillebrands and K. Ounadjela (Springer Verlag, Heidelberg, 2002), p. 27.
[33] P. Landeros, R. E. Arias, and D. L. Mills, Phys. Rev. B **77**, 214405 (2008).
[34] R. D. McMichael, D. J. Twisselmann, and A. Kunz, Phys. Rev. Lett. **90**, 227601 (2003).